Journal of Molecular Structure 1353 (2026) 144614

Contents lists available at ScienceDirect

Journal of Molecular Structure

journal homepage: www.elsevier.com/locate/molstr

Unveiling renaissance drawing techniques: A multimodal machine learning approach to the analysis of Giulio Romano's *Amazzonomachia*"

Claudia Scatigno [a,*], Silvia Giampaolo [a], Gabriella Pace [b], Serena Galetti [b], Maura Picciau [b], Giulia Festa [a,*]

[a] *CREF – Museo Storico della Fisica e Centro Studi e Ricerche Enrico Fermi, Via Panisperna 89a c/o Piazza del Viminale 1, 00184 Rome, Italy*
[b] *ICG – Istituto Centrale per la Grafica, Via della Stamperia 6, 00187 Rome, Italy*

ARTICLE INFO

Keywords:
Spectral signatures
Machine learning in art drawing conservation
Spectroscopy
Data fusion

ABSTRACT

During the Italian Renaissance, drawings were primarily created as preparatory studies for final works, including sculptures, paintings, and frescoes. Today, these drawings not only illustrate the conceptual and technical processes employed by artists but also enhance our understanding of the materials and techniques of the period. The analysis of such drawings involves execution methods such as strokes, line drawing, shading, and hatching, while also offering valuable insight into the development of art prints during that period. In this context, advanced technologies, such as spectroscopy and machine learning (ML) have been successfully employed to access the state of conservation, raw materials and execution methods of these masterpieces. Spectroscopy enables the identification of pigments, inks, and papers, while machine learning models can enhance the interpretation of complex data, revealing deeper insights into artistic processes, material degradation, and the evolution of drawing techniques.

Here, an innovative machine learning approach is developed for the analysis of composition, degradation, and artistic techniques of an Italian Renaissance drawing attributed to *Giulio Romano*, titled *Amazzonomachia* (16th century) and preserved at the *Istituto Centrale per la Grafica* in Rome. By integrating multimodal spectroscopic data (e.g. X-ray fluorescence spectroscopy - XRF, Fourier transform infrared spectroscopy - FTIR) with machine learning models, we identify the use of lead-based mine as the preferred workshop drawing material, and the use of iron gall ink to emphasize line strokes, providing valuable insights into the preservation and restoration of these masterpieces.

The results demonstrate a robust multimodal framework for analyzing historical drawing by integrating spectroscopy and machine learning, establishing a potential new standard in the field. The approach bridges material science and heritage studies, pushing cultural heritage diagnostics into the AI era.

1. Introduction and aim

Preparatory drawings provide a compelling insight into the creative process, offering a detailed examination of the artistic intentions and techniques that underpin the development of completed works of art [1–5]. The tradition of preparatory drawing began in the 15th century, when paper became more widely available. This made it easier for artists to use drawing as a way to plan and improve their ideas. From then on, drawing became a key section of artistic practice in Europe, helping authors get ready for commissions and try out parts of their future artworks. Within this context, Italian Renaissance artists adopted drawing as a crucial medium to explore and develop two fundamental aspects of their creative process: invention and draughtsmanship/design. By identifying key features and highlighting stylistic patterns, machine learning techniques overcome the constraints of conventional methods. The use of machine learning to understand artistic creativity through the analysis of historical drawings, including preparatory sketches, is still a relatively underexplored field. Pattern extraction and recognition through deep learning and computer vision in visual arts are recent tools of applications [6,7]. Studies have highlighted the effectiveness of machine learning methodologies in interpreting patterns, particularly within spectroscopic data [8–10]. Macro XRF scanning, μ-Raman

* Corresponding authors.
E-mail addresses: claudia.scatigno@cref.it (C. Scatigno), silvia.giampaolo@cref.it (S. Giampaolo), gabriella.pace@cultura.gov.it (G. Pace), serena.galetti88@gmail.com (S. Galetti), maura.picciau@cultura.gov.it (M. Picciau), giulia.festa@cref.it (G. Festa).

https://doi.org/10.1016/j.molstruc.2025.144614
Received 1 September 2025; Received in revised form 21 October 2025; Accepted 30 October 2025
Available online 31 October 2025

spectroscopy, and optical microscopy, combined with the spatial distribution of clusters and their mean spectra, reveal information about the painting sequence and materials [11]. Multimodal processes based on convolutional neural networks (CNNs) are used to classify paintings and artworks [12]. However, existing approaches often focus on specific methodologies or classification tasks, rather than on predicting the overall artistic style of an entire production [13]. The Renaissance period, particularly the Italian Renaissance, is a subject of enduring relevance and scholarly-academy interest [14].

This study aims to develop and validate an innovative multimodal framework that combines advanced spectroscopic techniques with machine learning algorithms to analyze the composition, degradation, and artistic techniques of the Italian Renaissance drawing *Amazzonomachia* (16th century), attributed to *Giulio Romano* and preserved at the *Istituto Centrale per la Grafica* in Rome. The objective is to enhance our understanding of Renaissance draftsmanship while providing concrete tools for conservation and restoration practices.

The methodology proposed is as follows: first, macroscopic observations are carried out to identify different areas of the drawing and address conservation-related questions, providing a crucial foundation for targeted restoration efforts. To investigate the execution techniques and offer concrete answers regarding the materials and methods used in the Renaissance workshop, an experimental campaign was conducted employing complementary, non-invasive, and non-destructive spectroscopic techniques, including XRF and FTIR. These tools are particularly well-suited to the analysis of historical drawings, where the presence of layered and fragile materials limits the application of traditional methods.

Machine learning models are then applied to analyze spectroscopic data, enabling the detection of subtle differences in spectral signatures that would otherwise remain indistinguishable. This allows for the identification of specific pigments and inks, even in overlapping or micrometer-thin layers. Through the extraction of spectral features, the methodology successfully identifies key materials (such as lead-based mine and iron gall ink), execution techniques (e.g., line drawing, shading, hatching), and evidence of material degradation or alteration processes.

The study employs a robust data fusion strategy based on Principal Component Analysis (PCA) concatenation of FTIR and XRF spectroscopic data. This multiblock approach allows for the joint analysis of complementary elemental and molecular information, enhancing pattern recognition and classification capabilities. By reducing dimensionality while preserving variance across modalities, the fusion of PCA scores enables the extraction of correlated features that reveal complex connections between materials and degradation phenomena. This integrated analysis facilitates a more comprehensive understanding of the drawing's composition, techniques, and conservation state further beyond what single-modal analysis would provide.

2. Experimental methods

2.1. The Giulio Romano drawing

The *Amazzonomachia* drawing is attributed to *Giulio Romano* belongs to the *Fondo Corsini, Gabinetto delle Stampe* collection, and it is preserved at the Central Institute for Graphics (inventory number FC124151 – deposit of the *Accademia dei Lincei*). The drawing was produced on a rectangular paper support (266 × 855 mm), with all four margins trimmed. The graphic signs were executed using brown ink, pen, watercolor applications, and graphite. This drawing holds significant historical and artistic value and has previously been identified as a preparatory study for the fresco executed in the *Sala delle Aquile* at the *Palazzo Te* in *Mantova*. Some scholars also suggest that it may belong to the circle of *Polidoro da Caravaggio*.

From a conservative point of view, the drawing shows paper and ink damage, notable signs of degradation and previous restoration treatments. Chromatic and physical alterations are observed such as surface deposits and incoherent particles, deformations, and foxing stains dispersed across the entire surface. Notably, a large brown stain is present, extending from the right margin inward into the drawing (approximately 16 cm in length). The drawing has undergone a previous restoration, which included reinforcements of paper sheets with Kozo-fiber veil (two of which are very extensive) and the repair of numerous *lacunae*. Moreover, it is likely that a deacidification treatment involving carbonates was carried out. The removal process of these added parts would not only represent a significant achievement in methodological procedure but also offer an invaluable opportunity for a comprehensive technical and scientific analysis of the artwork. The drawing is part of the *Restituzioni* restoration project, twentieth edition, one of the most prominent initiatives of *Progetto Cultura* [15], which has facilitated the restoration of over 2000 artworks across various periods and techniques.

2.2. Spectroscopic measurements

X-Ray Fluorescence (ED-XRF) and Fourier transform infrared (FTIR) spectroscopies were carried out for a total of 199 spectra acquired [16–17]. The selected measurement points are reported in the *Supplementary Information*, Figures S1-S2.

ED-XRF. The ED-XRF spectroscopy is performed using the XRaman spectrometer (Bruker) [16], with a Rhodium Target X-ray tube operating at 50 kV and 200 mA, with each acquisition time of 70 s. The system is equipped with a large-area Silicon Drift Detector (SDD) that has an active area of 25 mm^2 and an energy resolution of <135 eV at the MnKα line (5.890 eV). This setup enables the elements detection of with atomic numbers greater than 11 (sodium, Na), with an input photon rate of up to 100.000 counts per second. The collimator has been selected at 0.5 mm. A total of 151 spectra is recorded. The setup was the same for all measurements and normalization procedures are not applied to the entire dataset. The spectra are processed via Phyton using the software-environment Colab notebook 6.5.1 (Jupyter Notebook service) [18].

t-FTIR Spectroscopy. FT-IR spectra are recorded using a NICOLET iS5 spectrometer (Thermo Scientific, Waltham, Massachusetts, USA) equipped with a DTGS detector and a KBr beam splitter [17]. The spectra are sequentially collected over the range of 4000 cm^{-1} to 400 cm^{-1}, with 128 scans at a resolution of 2 cm^{-1}, resulting in a total of 48 spectra in t-FTIR (% Transmittance) [19]. All measurements are conducted under similar experimental conditions, without applying the second derivative of FTIR spectra [10]. The spectra are processed using the software-environment Colab notebook 6.5.1 (Jupyter Notebook service) [18].

Optical Investigations. Optical investigations were carried out for each point using a digital microscope (USB Microscope Jiusion) for surface observation with a maximum magnification of 1000 × and a resolution of 1920 × 1082 p Through microscopic analysis, it is possible to identify critical areas of interest, providing essential insights that support conservators and restorers in guiding their treatment strategies.

2.3. Machine learning analysis

The heterogeneous and multilayered nature of many advanced materials leads to significant chemical heterogeneity, which is reflected in complex spectral signatures. These spectra often contain overlapping vibrational features arising from multiple coexisting phases or components, making interpretation challenging. Moreover, degradation of the original materials contributes to increased spectral complexity, due to the formation of secondary compounds and alteration of functional groups. Unsupervised machine learning techniques, such as clustering and dimensionality reduction, provide powerful, data-driven approaches to uncover latent patterns and groupings within such complex datasets, without the need for prior labeling or reference data. Here,

unsupervised approaches are therefore more appropriate to enable the identification of intrinsic patterns and groupings within the data without relying on external labeling. This is particularly advantageous when dealing with heterogeneous or poorly characterized materials, as is often the case in the analysis of historical or altered objects. In this sense, the application of statistical methods can provide valuable insights into the drawing features and color distribution finalized to the understanding of the weight contribution of the different parameters such as brushstroke technique, use and distribution of ink throughout the entire drawing, pigments employment. Here, Principal Component Analysis (PCA) is used to highlight areas attributed to the original creation of the drawing, as distinct from those affected by aging or later modifications. Given the complexity of the object, which is stratified and composed of multiple layers, including original painting and subsequent additions (both pictorial and paper-based), the raw FTIR dataset was first analyzed. The loading reveals which elements such as pigment choice or shading style have the highest impact on the overall stylistic descriptions, allowing for a deeper understanding of the technical choices made by the artist.

The scores analysis identify different groups that correspond to different components, supporting their categorization and comparison. The analyses computed on the XRF data matrix allow to extract information related to a specific execution technique, supporting and confirming previous results, as well as providing insights into prior treatments. Distribution analyses, as well as clustering, give us indications regarding the use of a particular product and even the methods of application.

In this regard, a Python code has been developed for this investigation, specifically aimed at highlighting even the smallest differences. In detail, machine learning analyses were carried out through dedicated scripts developed via software environment Colab notebook 6.5.1 (Jupyter Notebook service) [18].

Several algorithms were computed and are reported in the following.

a. The FTIR data matrix is structured in two data matrixes: a 47 × 14,935 matrix that does not include standard analytes, and a 50 × 14,935 matrix that incorporates them for subsequent use in score evaluation. In this context, two Principal Component Analyses (PCA) were performed—both mean-centered—followed by score and loading evaluations. For each PCA, an optimal number of three components was identified, cumulatively explaining 97 % of the total variance. The variance distribution among the first two principal components showed slight differences between the two datasets: for the 47 × 14.935 matrix, PC1 explained 92 % and PC2 3 % of the variance; for the 50 × 14.935 matrix, PC1 accounted for 93 % and PC2 for 2 %. PCA provides a visual representation of the correlation between samples and variables, showing which variables influence the data samples or how they differ from each other. It is an unsupervised machine learning technique where features are assigned via successive clustering process based on measures of the variance data distribution distance.
b. The XRF data matrix is described by 151 × 3997 entries**.** Here, a Kernel Density Estimation (KDE) function was applied. It is a non-parametric method used to estimate the probability density function of a continuous random variable from a set of observed data. The main concept is smoothing the data by a kernel function, which produces a continuous estimate of the underlying probability distribution.

   The curve represents the distribution of a dataset by summing individual kernels (typically Gaussian) placed at each data point, with each kernel contributing to the overall density estimate. The KDE curve provides a visual alternative to histograms and is useful for identifying the underlying structure and features of the data, such as multimodality or skewness. The shape and smoothness of the curve are influenced by the bandwidth parameter, which controls the width of the kernels. An Agglomerative Clustering with 2 clusters and 'ward' linkage was also applied. A hierarchical clustering method that builds a hierarchy of clusters by starting with each data point as a single cluster and iteratively merging the closest clusters until the desired number of clusters is reached or all points are in a single cluster. Clusters = 2 specifies that the data are grouped into 2 clusters; linkage = 'ward' defines the method used to determine the distance between clusters. Ward linkage minimizes the variance within clusters, leading to more compact clusters. The number of clusters and the method of linkage have resulted from a cluster mapping and accuracy calculation. Additionally, a Principal Component Analysis (PCA) (mean-centered) with score and loading analysis was carried out. A total of two optimal numbers of components explained a total variance for each PCA (total of variance cumulated: 93 %, PC1 89 %, PC2 4 %).

a. FTIR and XRF data fusion. The fused dataset has a shape of 44 × 18,932. 44 represents the number of measurement points (MPs) that are common and aligned between the FTIR and XRF datasets after preprocessing. 18,932 represents the total number of features (variables) resulting from the horizontal concatenation of the FTIR and XRF datasets. This includes the spectral variables from FTIR and the elemental information from XRF, combined feature-wise into a single matrix. In detail, the principal components extracted from the FTIR and XRF data were fused by concatenating the dataframes side-by-side.

   The fused data matrix representing the combined spectral information from both analytical techniques. These steps provide a solid foundation for subsequent multivariate analysis of the fused data. A workflow chart is reported below, in the Fig. 1.

3. Results and discussion

Analysis of the FTIR spectra reveals significant differences in both the shape and intensity of absorption bands, indicating potential variations in molecular structure or intermolecular interactions within the sample. Several prominent vibrational signals appear to be masked by overlapping bands, indicating the presence of multiple components. While second-order derivative FTIR spectra are commonly used to resolve such overlaps [20], this approach was not employed. Instead, Principal Component Analysis (PCA) was applied directly to the raw FTIR dataset to highlight subtle spectral differences, distinguish co-existing materials, identify characteristic patterns, and reveal underlying structures.

In this context, the loading plot (Fig. 2) shows enhanced band resolution, aiding in the identification of compounds masked by overlapping signals in the raw spectra. Analysis of the loading plot indicates the presence of spectral regions consistent with the absorption profiles of lipid compounds and historical components commonly found in traditional iron gall ink formulations (Fig. 2). Under microscopic examination, specific areas and line features of the drawing appear to be compatible with the materials identified through spectroscopy (see Supporting Information). The PC2 component shows that approximately 3 % of the data exhibit benchmark spectroscopic absorption bands, notably the characteristic bands at 3010, 2923, and 2853 cm^{-1} corresponding to C–H stretching vibrations, and the band at 1746 cm^{-1} attributed to carbonyl groups in glycerol ester linkages (Table 1). This latter band is otherwise overlapped by signals from carbonyl groups in carboxylic acid functionalities. Other spectral regions, such as the range from 1460 to 400 cm^{-1} (labelled with 3, shaded area in Fig. 1), are difficult to detect in FTIR spectra due to lower absorption intensity and variability. Similarly, the band at 723 cm^{-1} (labelled with n.4), which corresponds to cis (C–H) out-of-plane deformation, is also challenging to observe [20]. However, the loading plot is nonetheless capable of extracting relevant information from these regions, highlighting subtle but significant spectral features (Fig. 2).

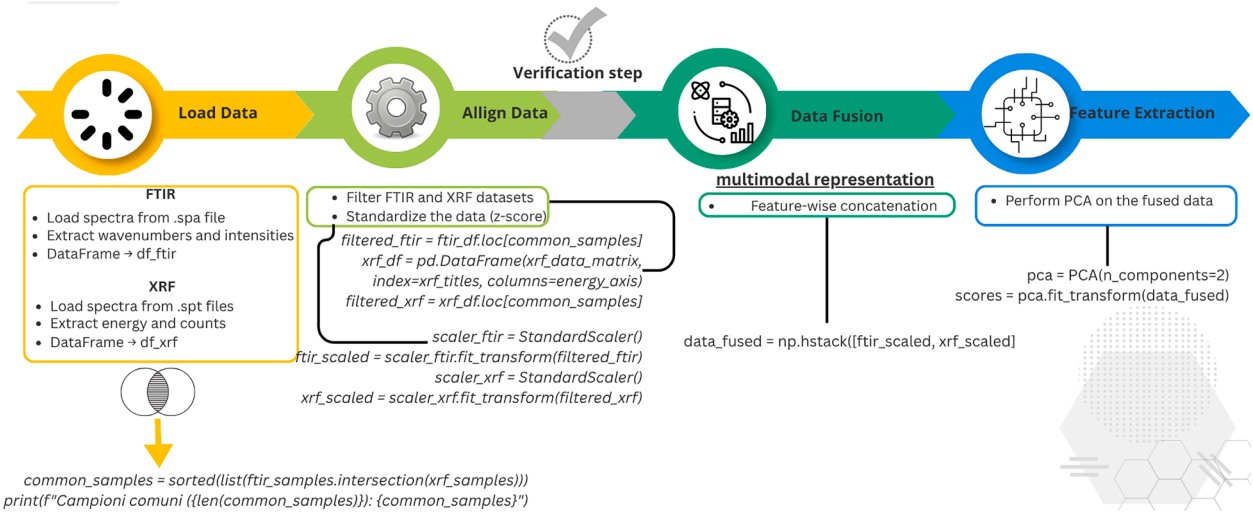

Fig. 1. Multimodal Spectroscopic Data Fusion workflow: FTIR+XRF+PCA-based. The analysis begins with data loading, where raw FTIR and XRF datasets are imported. Next, feature extraction is performed to select relevant variables and reduce dimensionality. Following this, data alignment ensures that samples from both datasets correspond correctly by matching common samples and ordering. Finally, data fusion integrates the aligned and preprocessed FTIR and XRF features into a single combined dataset, enabling comprehensive multivariate analysis such as PCA.

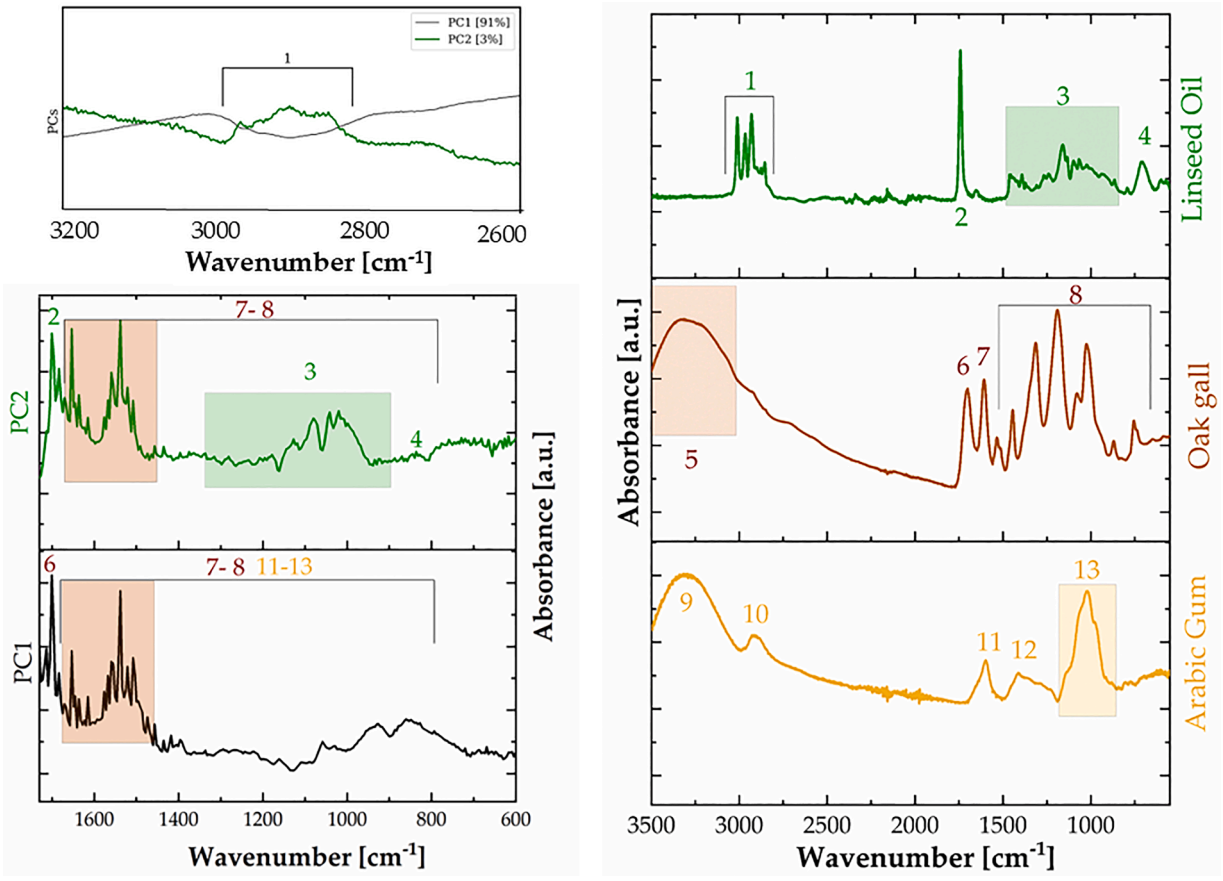

Fig. 2. Loading plots [47] and spectra of standard samples such as linseed oil, oak gall and Arabic gum.

PC2 also shows a residual signal related to the constituent material [20] such as iron gall ink. In contrast, 91 % of the data reflect only the typical constituent materials of the drawing under investigation [20].

The score plot (Fig. 3) illustrates the relation between measurement points (MPs) based on the variance in spectral distribution across frequencies, effectively clustering the MPs according to the specific variance associated with certain molecular vibrations.

In addition to the 47 measured points, the matrix also includes 3 standard spectra—representing linseed oil, oak gall, and Arabic gum, as references to examine the characteristics of the oily substance and the ink execution techniques.

The total variance explained reaches 97 %, with the first principal component (PC1) accounting for 93 % of the data distribution. Most of the data shows similar molecular composition, suggesting that the same

Table 1
Assignments of the IR absorption bands evidenced by the loading plot of PC1 vs PC2 as illustrated in Fig. 1. STD=standard samples.

n.	Wavenumber [cm^{-1}]	Functional Group	Note
1	3010, 2923, 2853	νCH_3-CH_2	STD* [20–21]
2	1742	νC=O	STD* [20–21]
3	1461–798	fingerprint	STD* [20–21]
4	721	cis (C-H) out-of-plane deformation	STD* [20–21]
5	3600–3000	νOH, phenolic compounds	STD** [9, 22–23]
6	1700	C=O, hydrolyzable tannins	STD** [9, 22–23]
7	1600	aromatic ring, condensed tannins	STD** [9, 22–23]
8	1100–1000, 880–870, 770–750	fingerprint tannins	STD** [9, 22–23]
9	3220	νOH, phenolic compounds	STD*** [24]
10	2919	νC–H	STD*** [24]
11	1604	δOH	STD*** [24]
12	1426	νC=O	STD*** [24]
13	1143, 1050, 1015	νsym. and νasym. C– C–O, C–O–C	STD*** [24]

STD*: Linseed Oil purchased from [21].
STD**: Oak Apples purchased from [22].
STD***: Gum Arabic Powder purchased from [24].

technique was used throughout the drawing. The high percentage of variance associated with the first component demonstrates that the drawing indeed exhibits the co-presence of materials that differ compositionally. The variance associated with the residuals, which account for around 2 % of the data, is linked to PC2. Along this axis, non-original areas are distributed, including regions where the molecular fingerprint is dominated by additional materials, such as retouches or additions. In this case, the score plot reveals two main groupings: the positive side of PC2 (covering the first and second quadrants) and the negative side of PC2 (covering the third and fourth quadrants). The former corresponds to the retouched areas, while the latter corresponds to the original areas of the drawing. In detail it is possible to highlight:

a) MPs belonging of retouching areas (I)
b) MPs corresponding to oily spots (II)

Further details are shown in the Supporting Information (Figure S3).
c) MPs measured in areas with colored dots and pencil stroke are present (III). Further details are shown in Supporting Information (Figure S4) d) MPs in quadrant IV reports points measured in areas with dark-medium black ink associated with the execution ink.

A clear trend along PC1 can be observed. For example, in quadrant IV, the ink stroke changes, points shift from left to right in a way that corresponds to an associated color gradient, from dark to lighter areas, almost white. This distribution is highlighted by the gray arrow in the figure, which shows the change from left to right (Supporting Information, Figure S5). The ink reveals a broad range of effects, from fine lines to darker, more intense strokes, suitable for both technical drawings and expressive, artistic interpretations.

The Score provides further insights. The points measured on the *verso* (reported in red in Fig. 3) are all clustered in quadrant II, except for P149 that is located but in an oily spot region. As suggested by the restorers, a linseed oil standard has also been included in the matrix. The variance is consistent with the other points in quadrant II. It is also possible to deduce that this area involves the drawing on its right side and suggests it was "applied from the *verso*."

An analysis of the quadrant IV of the loading plot concerns the ink composition and reveals distinct vibrations associated with oak galls and gum Arabic [9,22–23]. Moreover, it is possible to confirm the findings from the FTIR analyses and extract additional information, potentially hidden, located in specific areas or points of the preparatory drawing.

The elemental analysis enabled the identification of the predominant elements and traces associated with the various layers of the preparatory drawing. Several key elements are detected such as sulfur (S), potassium (K), calcium (Ca), titanium (Ti), iron (Fe), and zinc (Zn). As an example, Fig. 3 reports the XRF spectra that corresponds with the entire dataset. Sulfur and iron are particularly significant in the composition of iron-gall ink. In traditional formulations, iron typically originates from iron (III) sulfate ($Fe_2(SO_4)_3$) or iron (II) sulfate ($FeSO_4$). The dark ink color results from the reaction between iron salts and tannins in the oak galls. Sulfur is present as sulfate ions (SO_4^{2-}), which derive from the iron sulfate ($FeSO_4$) used in the ink formulation. Sulfur plays a crucial role in stabilizing the iron-tannate complex those forms within the ink. It is also shown in Fig. 3 that the Fe/S ratio is different, suggesting that the ink was used in a different manner in the execution of the artwork. Details are reported in Supporting Information, Figure S3. Cinnabar, a pigment consistent with historical palettes of the period, was also identified. However, its localized occurrence suggests an incidental presence rather than intentional use.(Fig. 4)

Moreover, a lead-based mine has been identified in the drawing corresponding to P35, P36, P37, and P63. Upon examining the color fill, even at magnifications using an optical microscope (ochre-orange hue), it is attributed to a lead mine [25]. This is supported by literature, where lead mine is frequently cited as a material of choice in preparatory drawings due to its high visibility and good adhesion to different types of support [26]. The presence of lead is particularly abundant in certain

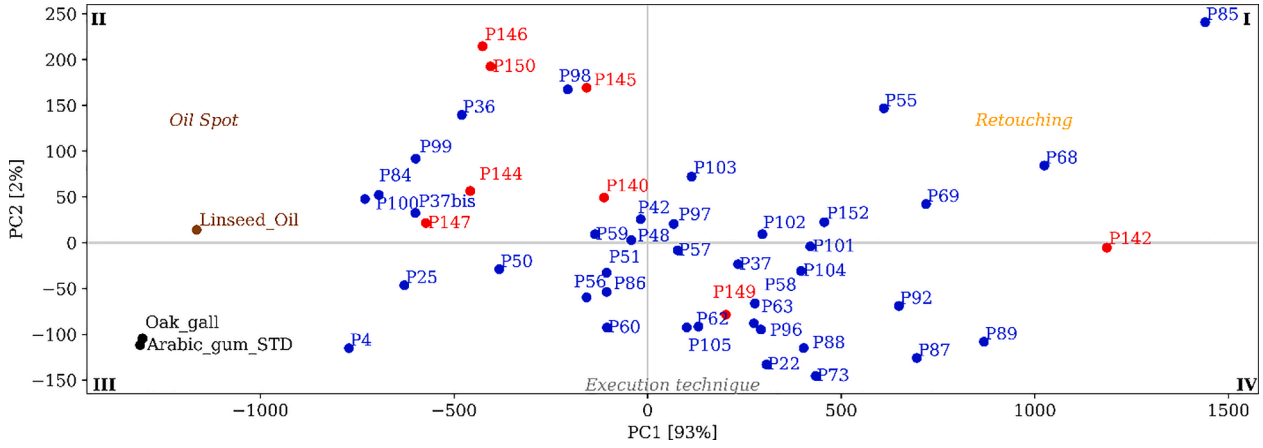

Fig. 3. Principal Component Analysis (PCA) score plot of FTIR spectra [50 × 14,935]. Measurement points (MPs) are displayed in two colors, corresponding to their respective groups: blue for points measured on the recto side and red for points measured on the verso side. The plot further highlights the PCA quadrants using Roman numerals (I, II, III, IV), following the anti-clockwise direction.

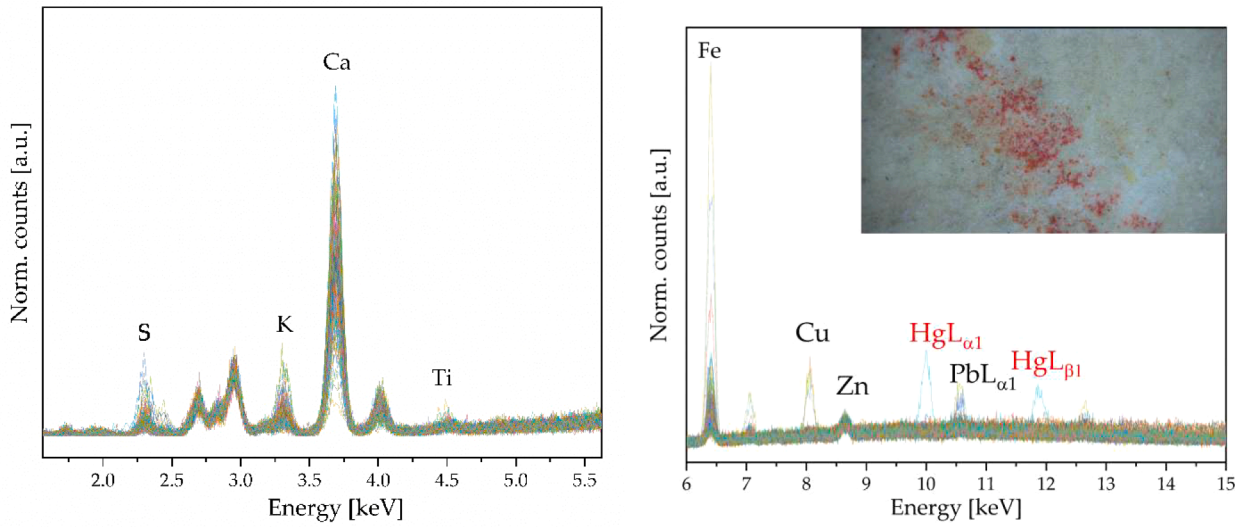

Fig. 4. XRF dataset composed by 151 spectra. The labeled peaks correspond to the Kα₁ emission lines, except for mercury (Hg) and lead (Pb). Mercury (Hg) is detected only in P151, and it is associated with cinnabar. Isolated occurrences of copper (Cu) and lead (Pb) are also observed.

areas of the preparatory drawing. This suggests the use of this element in specific areas intended by the artist and contextually relevant to the historical period of the manufact [26]. Fig. 5 shows how the use of a lead pencil was specifically employed to define strokes and create contour lines. It is also noticeable that the amount used to execute these lines/strokes is the same. This suggests that the execution of these lines occurred simultaneously. This is equally consistent with what has been found in the literature: in the context of preparatory drawings, lead mines were often used to delineate contours, define composition, and plan the distribution of colors in realistic drawings [26–29]. As a light-resistant and relatively stable material, it allowed artists to leave enduring marks on which they could build over extended preparatory stages [26–29].

Furthermore, XRF data was used to evaluate the abundance of calcium (Ca) [30]. It has various sources primarily due to the composition of the paper itself and to specific treatments during production processes. Another reasonable source concerns restoration processes where the calcite was produced during the acidification process with the application of $Ca(OH)_2$ in semi-saturated solution. Fig. 6 displays a single Kernel Density Estimation (KDE) curve, which provides the overall distribution of Ca intensities across all 151 spectra, which corresponds to the most frequent or typical Ca intensity and shows the variability or spread of Ca values across the spectra. Observing the curve, the spread is narrow, reflecting relatively low variability in Ca across the measurement points. Notably, the curve exhibits multiple distinct peaks, which could suggest the presence of subgroups or clusters within the data, each with different calcium intensity characteristics. In detail, Fig. 6 shows a roughly symmetric curve, which suggests a normal, bell-shaped distribution of Ca intensities, with a tendency towards higher Ca values. The curve is slightly skewed to the right (a tail on the right side), indicating a higher frequency of measurement points with elevated Ca intensities. Additionally, a few outliers are observed in the

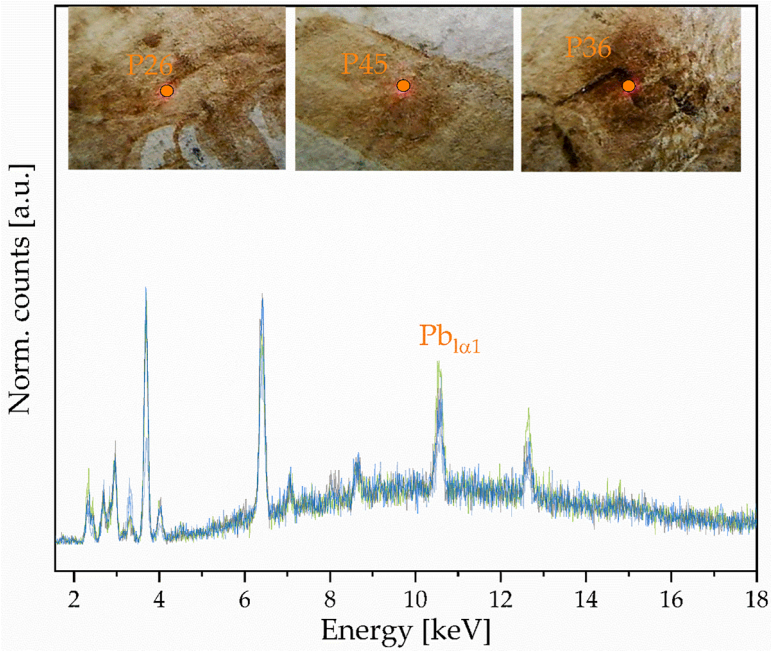

Fig. 5. XRF spectra of the P35, P36, P37, and P63 measurement points are attributed to the lead-based mine.

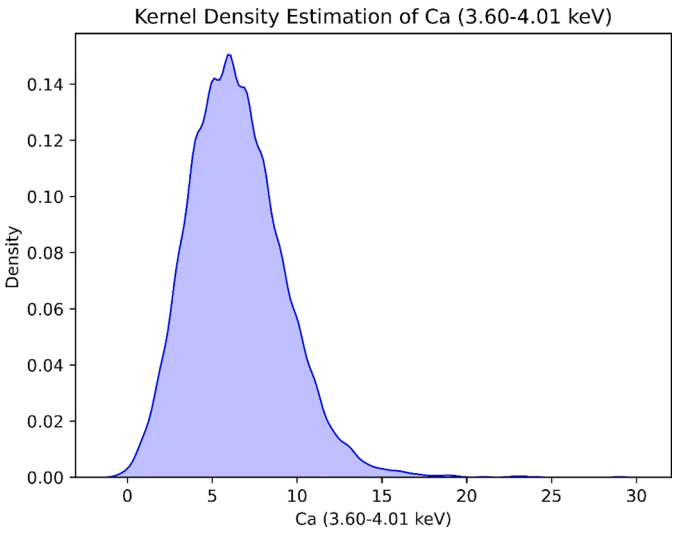

Fig. 6. Kernel Density Estimation (KDE) of Ca signal in the range of 3.60–4.01 keV along 151 measurement points from P1 to P151. The x-axis represents the values of normalized counts in the range of 3.60–4.01 keV attributed to the Ca signal. Y-axis: Density. It indicates the probability density of the calcium values across all points. Higher density values correspond to regions where certain intensity values are more likely to occur, reflecting areas of greater concentration in the distribution.

distribution, as some points fall well outside the main body of the curve.

To gain a deeper understanding of the element distribution across the drawing, a score plot is computed, accompanied by an agglomerative clustering approach (Fig. 7).

The score plot with agglomerative clustering reveals an elemental distribution characterized by two major clusters. Sulfur and iron, which once again define the two primary elemental categories associated with the execution technique and the use of iron-sulfur based ink, are clearly distinguished. The two clusters highlight the trends of Fe and S elements, which, for certain points in the investigated preparatory drawing, exhibit particular abundance. Specifically, points labeled as P132, P78, P85, P83, P27, and P21 are particularly enriched in S, as described by PC1 with high variance. Along with PC2, the other element that differentiates the remaining points is Fe. By examining the measurement points with lower variance, additional subcategories, such as integrative gaps characterized by specific elements such as copper, are identified. Details are reported in the Supporting Information, Figure S6.

Fig. 8 presents the scores plot of Principal Component Analysis (PCA) applied to the fused FTIR and XRF datasets. The distribution of 44 samples is visualized in the two-dimensional space defined by the first two principal components (PC1 and PC2), which explain 66.47 % and 10.74 % of the total variance, respectively, resulting in a cumulative explained variance of 77.21 %. Each point corresponds to an individual sample, labelled by its identifier. A subset of samples =- highlighted in red =- is clearly separated from the main cluster - shown in bright blue =- indicating distinctive multimodal spectral characteristics. These samples notably correspond to areas measured on the verso side of the preparatory drawing. This fused representation reinforces and integrates patterns previously observed separately in Fig. 3 (XRF) and Fig. 6 (FTIR). For example, sample P85, collected from a lacuna subsequently filled during later pictorial restoration, is characterized by a high sulphur signal (Fig. 6) and appears here in the outer corner of the first quadrant, within the retouching area already highlighted in Fig. 3. In contrast, sample P25 lies on the opposite side of the plot, consistent with its iron-rich composition (Fig. 6) and its association with the original execution technique involving gallnut ink and Arabic gum. Data fusion further enabled the identification of subtle differences that were not apparent when the datasets were analysed independently. Sample P98, although located on the verso and coinciding with an oil stain, is grouped here with samples associated with the original sketching activity, suggesting that its spectral signature is more closely related to that material context than to the oil contamination. Additionally, the fusion analysis reveals a clear difference between samples P4 and P25, which in previous analyses (Figs. 2 and 6) appeared closely associated with the same original application technique. In the fused PCA space, however, their divergence can be related to subtle variations in how the sketching material was applied: P25 is associated with more continuous and fluid strokes, whereas P4 shows evidence of a coarser and less regular application. This differentiation is further supported by visual inspection, as shown in Supplementary Figure S4.

4. Conclusions

The capability to analyze layered materials represents a breakthrough in art conservation. The combination of X-ray fluorescence spectroscopy, Fourier-transform infrared spectroscopy, and machine learning offers a comprehensive, multimodal framework for analyzing complex artworks, revealing hidden patterns and processes that were previously undetectable with traditional methods. This study demonstrates the effectiveness of advanced spectroscopic techniques coupled with machine learning (ML) for the analysis of ancient drawings. This innovative methodology was applied to a *Giulio Romano* preparatory drawing named *Amazzonomachia* (16th century). Significant insights were obtained in terms of materials and techniques employed by the artist. The identification of lead-based mine as drawing material to define stroke and lines and the use of iron gall ink for the signs provide a deeper understanding of the artistic processes. Additionally, cinnabar, a pigment consistent with historical palettes of the period, was also identified. However, its localized occurrence suggests an incidental presence rather than intentional use. The identification of linseed oil in specific areas and copper-based spots is also crucial for determining the restoration procedure that will be applied enabling conservators to accurately carry out the necessary interventions.

In conclusion, this study demonstrates the effectiveness of integration of spectroscopic techniques with machine learning provides a powerful tool for art historians and conservators to unlock new layers of information, offering a more nuanced understanding of Renaissance artworks and guiding future conservation efforts. This research presents a new paradigm for art historical and conservation analysis, pushing the boundaries of how we study, interpret, and preserve cultural heritage. The integration of spectroscopic data with machine learning techniques has become standard practice in the field. While the use of spectroscopy and machine learning in heritage science is well-established, recent advances lie in how these tools are applied to provide more accurate insights into the materials and techniques used in historical art. Moreover, the data fusion of FTIR and XRF spectra proved effective in uncovering subtle material and structural differences that were not identified through the individual techniques alone, thus enabling a deeper interpretation of the drawing's layered composition and execution technique.

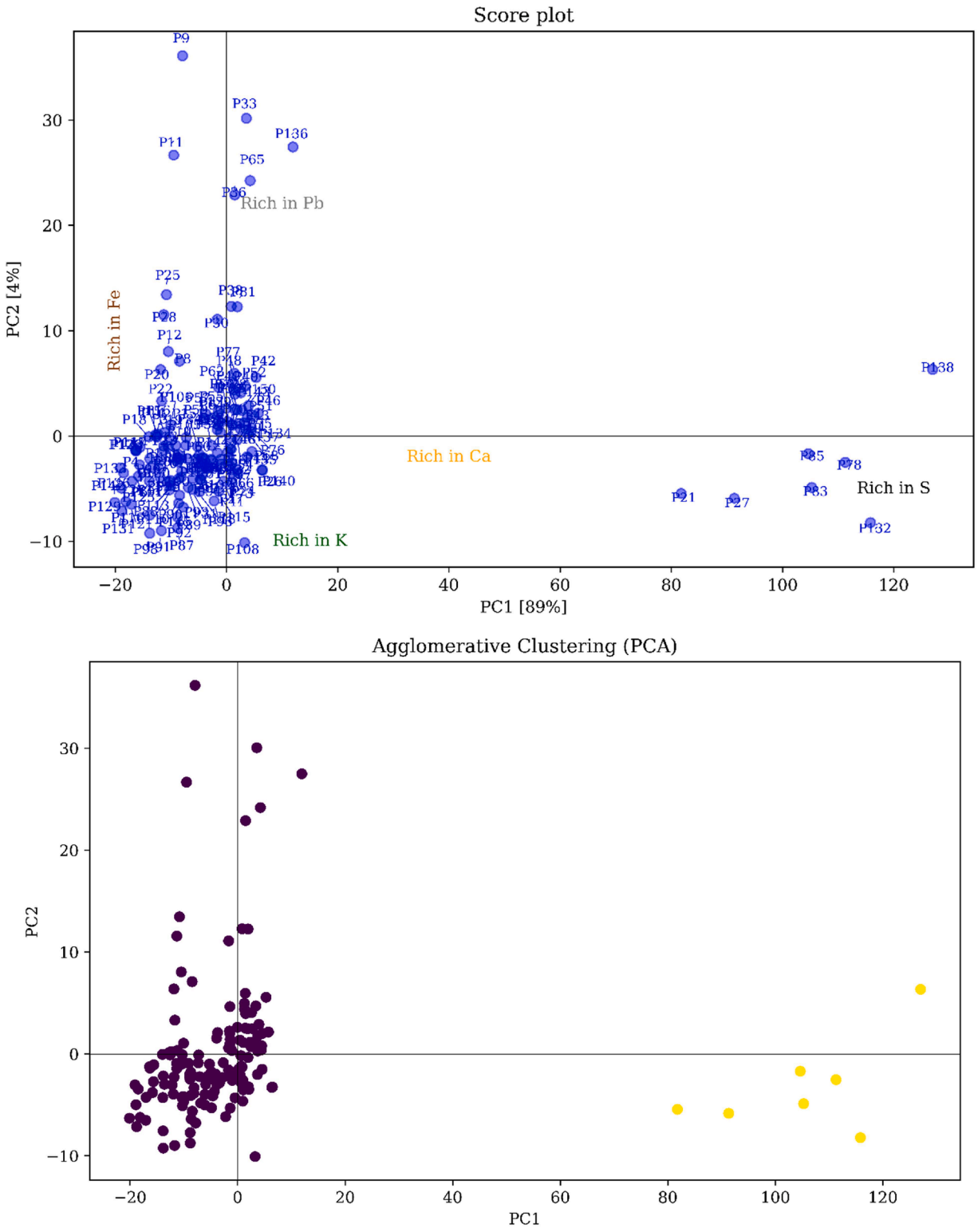

Fig. 7. Score plot (top) of the XRF spectra [151 × 3997 entries] and agglomerative clustering results (bottom).

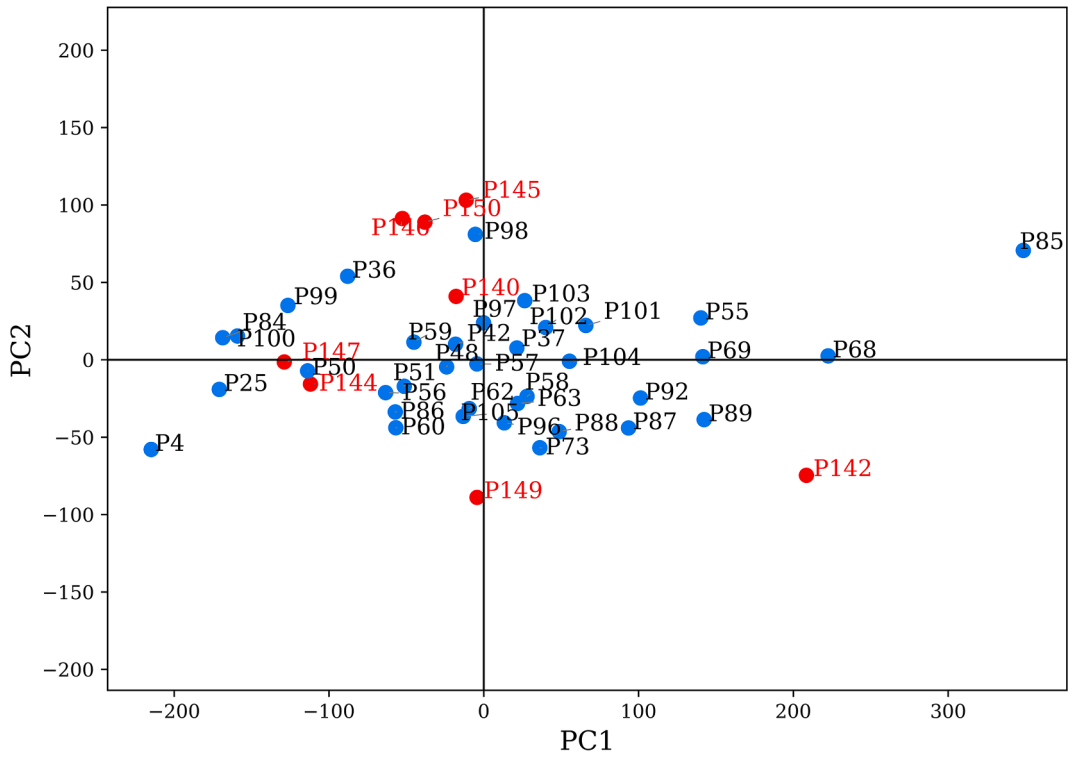

Fig. 8. Fused FTIR+XRF data frames by PCA. Data Matrix shape: (44, 18,932).

Foundings

This work was supported by the CREF - Museo Storico della Fisica e Centro Studi e Ricerche Enrico Fermi founding in the framework of the Physics for Cultural Heritage research group.

CRediT authorship contribution statement

Claudia Scatigno: Conceptualization, Methodology, Software, Validation, Formal analysis, Investigation, Data curation, Writing – original draft, Writing – review & editing, Visualization. **Silvia Giampaolo:** Investigation, Data curation, Writing – review & editing. **Gabriella Pace:** Resources, Data curation, Project administration, Writing – review & editing. **Serena Galetti:** Investigation, Data curation, Writing – review & editing. **Maura Picciau:** Writing – review & editing. **Giulia Festa:** Conceptualization, Methodology, Investigation, Resources, Data curation, Writing – review & editing, Supervision, Project administration.

Declaration of competing interest

The authors declare that they have no known competing financial interests or personal relationships that could have appeared to influence the work reported in this paper.

Supplementary materials

Supplementary material associated with this article can be found, in the online version, at doi:10.1016/j.molstruc.2025.144614.

Data availability

Data will be made available on request.

References

[1] L. Nuti, Surveying, interpreting, and designing: the multiple essence of a sixteenth-century drawing, J. Soc. Architectur. Historian. 75 (1) (2016) 5–24.

[2] F. Vermeylen, The function of the preparatory drawing in Italian renaissance painting, Burlingt. Mag. 147 (1227) (2005) 678–687.

[3] Rosemary E. Butcher, Collecting drawings: a Survey of the History of the Drawing collection: With a Proposal For an Exhibition of Sixteenth and Seventeenth Century Italian drawings' Rebirth in Baroque lines, University of St Andrews, 1993. PhD diss.

[4] P. Barolsky, Drawing and Design in the Renaissance: A contextual approach. Renaissance Quarterly, 54(4), 1093–1117; White, J. (1992). The preparation of drawings and sketches for large-scale compositions in the renaissance, Art J. 51 (1) (2001) 36–41.

[5] M. Bergstein, Drawing On the Right Side of the Brain: A Guide to Understanding the Techniques of Renaissance Masters, Harper Collins, 2013.

[6] G. Castellano, G. Vessio, Deep learning approaches to pattern extraction and recognition in paintings and drawings: an overview, Neural Comput. Applicat. 33 (19) (2021) 12263–12282.

[7] J. Qin, X. Sun, W. Xu, A state-of-art review on intelligent systems for drawing assisting, in: International Conference on Human-Computer Interaction, Springer Nature Switzerland, Cham, 2023, pp. 583–605.

[8] C. Scatigno, G. Festa, FTIR coupled with machine learning to unveil spectroscopic benchmarks in the Italian EVOO, Int. J. Food Sci. Technol. 57 (7) (2022) 4156–4162.

[9] G. Festa, M.S. Maggio, L. Teodonio, C. Scatigno, Ancient handwriting attribution via spectroscopic benchmarks and machine learning: 'Clavis Prophetarum' by Antonio Viera, Expert Syst. Appl. 227 (2023) 120328.

[10] C. Scatigno, L. Teodonio, E. Di Rocco, G. Festa, Spectroscopic benchmarks by machine learning as discriminant analysis for unconventional Italian pictorialism photography, Polymer. (Basel). 16 (13) (2024) 1850.

[11] S. Kogou, L. Lee, G. Shahtahmassebi, H. Liang, A new approach to the interpretation of XRF spectral imaging data using neural networks, X-Ray Spectromet. 50 (4) (2021) 310–319.

[12] A. Belhi, A. Bouras, S. Foufou, Leveraging known data for missing label prediction in cultural heritage context, Appl. Sci. 8 (10) (2018) 1768.

[13] J. Valencia, G.G. Pineda, V.G. Pineda, A. Valencia-Arias, J. Arcila-Diaz, R.T. de la Puente, Using machine learning to predict artistic styles: an analysis of trends and the research agenda, Artif. Intell. Rev. 57 (5) (2024) 118.

[14] https://news.artnet.com/art-world/google-arts-and-culture-leonardo-da-vinci-ai-2341473 (accessed on 11 April 2025). https ://w ww.meetcenter .it/en/ understanding-the-invisible-refik-anadol/.

[15] https://group.intesasanpaolo.com/en/newsroom/all-news/news/2023/Restitutions-program-protects-artistic-works (accessed on 9 January 2025).

[16] Available online: https://www.bruker.com/it/applications/academia-materials-science/art-conservation-archaeology/special-engineering.html (accessed on 11 April 2025).

[17] Available online: https://assets.thermofisher.com/TFS-Assets/CMD/brochures/BR-51983-nicolet-is5-ft-ir-spectrometer-D19549.pdf.
[18] Available online: https://colab.google/(accessed on 11 April 2025).
[19] Available online: https://www.thermofisher.com/order/catalog/product/869-188700?SID=srch-srp-869-188700 (accessed on 11 April 2025).
[20] Penelope Banou, Stamatis Boyatzis, Konstantinos Choulis, Charis Theodorakopoulos, Athena Alexopoulou, Oil Media on paper: investigating the interaction of cold-pressed linseed oil with paper supports with FTIR analysis, Polymer. (Basel) 15 (11) (2023) 2567.
[21] Available online: https://www.kremer-pigmente.com/en/shop/mediums-binders-glues/73020-linseed-oil-from-sweden.html (accessed on 11 July 2025).
[22] V. Corregidor, R. Viegas, L.M. Ferreira, L.C. Alves, Study of iron gall inks, ingredients and paper composition using non-destructive techniques, Heritage 2 (4) (2019) 2691–2703.
[23] Available online: https://www.kremer-pigmente.com/en/shop/dyes-vegetable-color-paints/natural-organic-dyes-vegetable-color-paints/37400-oak-apples.html (accessed on 11 July 2025).
[24] Available online: https://www.kremer-pigmente.com/en/shop/mediums-binders-glues/63330-gum-arabic-powder.html (accessed on 11 July 2025).
[25] Available online: https://www.jstor.org/stable/44064971?seq=1 (accessed on 28 January 2025).
[26] Francis. Nicholson, The practice of drawing and painting landscape from nature, in water colours: exemplified in a series of instructions calculated to facilitate the progress of the learner; including the elements of perspective, their application in sketching from nature, and the explanation of various processes of colouring, for producing from the outline a finished picture; with observations on the study of nature, and various other matters relative to the arts, J. Booth. (1820).
[27] S. Owens, The Story of Drawing: An Alternative History of Art, Yale University Press, 2024.
[28] J. Hassell, The Camera, Or, Art of Drawing in Water Colors: With Instructions For Sketching from Nature. The Whole Process Familiarly Exemplified in Drawing, Shadowing, and Tinting a Complete Landscape, in All Its Progressive Stages. With Directions For Compounding and Using Colors, Sepia, Indian Ink, Bister, &c, Simpkin, Marshall, and Company, 1845.
[29] H. South, The Everything Drawing Book: From Basic Shape to People and Animals, Step-by-step Instruction to Get You Started, Simon and Schuster, 2004.
[30] L. Teodonio, C. Scatigno, M. Missori, G. Festa, Late middle ages watermarked Italian paper: a machine learning spatial-temporal approach, J. Cult. Herit. 57 (2022) 53–59.